An approximation model for nonlinear wave induced moment on a vertical surface-piercing column

Xingya Feng[1], *P. H. Taylor*[2], *S. Dai*[3], *S. Day*[3] *and T. A. A. Adcock*[4]
[1]Department of Ocean Science and Engineering, Southern University of Science and Technology, Shenzhen, China
[2]Faculty of Engineering and Mathematical Sciences, University of Western Australia, Perth, Australia
[3]Department of Naval Architecture, Ocean and Marine Engineering, University of Strathclyde, Glasgow, UK
[4]Department of Engineering Science, University of Oxford, Oxford, UK

ABSTRACT

This study focuses on the analysis of the higher harmonic wave moments (around the seabed) on a vertical cylinder under the action of focused wave groups. The moment is known to be more nonlinear than the horizontal wave force; however, it is not very much investigated in the literature due to the difficulty of measuring accurately the mudline moment. We analysed the carefully measured wave loads from the tests in the Kelvin tank in the University of Strathclyde where a four-phase method is employed to extract the harmonic wave loads. The mudline moment shows a 'Stokes-like' underlying harmonic structure similar to the horizontal force. An approximation model is established to estimate the harmonic moment from the linear moment component. The model requires the nonlinear horizontal force coefficients and the moment arm of each harmonic. The moment arm for each higher harmonic is found from the measured forces and moments. The approximation model is demonstrated successful from both the measured data and numerical simulation.

KEY WORDS: Offshore wind; Monopile; Nonlinear loads; Higher harmonics; Focused waves.

INTRODUCTION

Large waves are usually expected during the operation of offshore wind turbines which are typically supported by bottom-mounted monopiles in relatively shallow waters. The typical Keulegan-Carpenter (KC) number for offshore wind turbine monopiles implies that inertia loading will dominate and viscous drag forces can be neglected. For non-breaking waves the dominant load will be at the same frequency as the incoming waves and can be well captured by a standard linear calculation. However, there will be higher harmonics to the loading by large waves and these can make up a significant part of the magnitude of the total loads. The higher harmonic loads will tend to act near the free surface and therefore have a higher moment arm than the linear loads – and hence increase moment loading on the foundations. However, not very much work has been seen in the literature that focuses on the investigation of the nonlinear moment on a vertical circular cylinder.

In a large amount of the work on the higher harmonic loads, researchers mostly focus on the horizontal wave force. This is partial because, importantly the higher harmonic force will potentially act at around the natural frequency for which an offshore wind turbine is designed for (see Kallehave et al. 2015). This is of obvious concern for structural and geotechnical design. This resonance is coupled with the well known problem associated with column-supported offshore structures which is the 'ringing' occurring at a substantially higher frequency than the dominant wave frequency. The ringing is known to be caused by nonlinear extreme waves exciting transient response at the structural resonant modes. The higher-harmonic ringing loads on a vertical surface-piecing cylinder have been observed in the offshore field and measured in laboratory experiments. The observations have been reported in a number of experimental studies (Davies et al., 1994; Krokstad and Stansberg, 1995; Chaplin et al., 1997).

Models for analyzing higher harmonic loads have been extended from linear theory to second and third orders. For example, Faltinsen, Newman and Vinje in Faltinsen et al. (1995), developed a third-order diffraction model (referred as FNV) for approximating the third-order wave force on a slender cylinder, based on the assumptions of deep water and that the incident wave amplitude is in the same order with the cylinder radius. The FNV model was shown to produce good prediction of the third-order force in its assumed regime in some recent experiments (Huseby and Grue, 2000; Chen et al., 2018; Kristiansen and Faltinsen, 2017). Malenica and Molin (1995) (referred as M&M) made a complete third-order diffraction analysis following the perturbation method and a semi-analytical solution for the third-order potential was presented. In a separate approach Rainey (1989) and Rainey (1995) derived a simplified expression for wave loads up to third order on a slender body in the perspective of fluid kinetic energy, without solving for the velocity potential. It also assumed an undisturbed incident wave field. The 'point load' component, Equation (4) in Rainey (1995), at the body-surface intersection was highlighted. It was explained by pressures inherently different from those elsewhere on the cylinder as a result of an 'end effect'. In the diffraction theory in Malenica and Molin (1995), this point load is a waterline integral on the still water surface-intersection.

This point load component could become dramatically important at higher harmonics. The point load at the third order also suggests that the higher (than second) order load might act close to the free surface.

In a recent experimental work in Riise et al. (2018a), high-frequency resonant response of a monopile in deep water irregular waves was studied, where the monopile is weakly damped such that the resonant motion can be captured. They measured the higher harmonic moments on the monopile by assuming the moment arm is the water depth, that is, the higher harmonic force acts exactly on the still water surface. They extracted the third, fourth and fifth harmonic force components from the irregular wave results and compared to the FNV model and other available experiments. They concluded that the irregular wave measurements can generalize results obtained in deep water regular waves.

In the present study, we use a focused wave group as the incident wave for representing a transient excitation. The experiments were carried out in the Kelvin Hydrodynamic Lab in the University of Strathclyde, UK. Both the horizontal wave loads and tank bottom moments were measured. The method for extracting higher harmonic responses from a focused wave group in our tests is the phase-manipulation based decomposition, recently used by Chen et al. (2018) for experiments and Fitzgerald et al. (2014) for numerical simulation. The approach assumes a 'Stokes-type' harmonic structure of both wave elevations and hydrodynamic forces for a narrow-banded wave group. We present here a similar 'Stokes-type' harmonic moment model with appropriate non-dimensionalization. With both the harmonic horizontal forces and and moment extracted from the measurement, we can find the acting location of each harmonic force and the moment arm. With the non-dimensionalized harmonic coefficients, following the 'Stokes-type' structure, we reconstruct the wave moment from the linear wave force, which can be easily obtained from linear diffraction theory.

METHODOLOGY

Decomposition model

We first present the decomposition model for the wave force. In the framework of potential flow, the fluid is assumed inviscid and incompressible and the flow irrotational. With the assumption of narrow-banded spectrum, the focused wave group has a slowly-varying amplitude $A(t)$ near focusing and the wave force is expanded with respect to wave steepness as

$$F(t) = A\mathfrak{F}_{11}\cos\varphi + A^2(\mathfrak{F}_{20} + \mathfrak{F}_{22}\cos 2\varphi) + A^3(\mathfrak{F}_{31}\cos\varphi + \mathfrak{F}_{33}\cos 3\varphi) + A^4(\mathfrak{F}_{40} + \mathfrak{F}_{42}\cos 2\varphi + \mathfrak{F}_{44}\cos 4\varphi) + O(A^5) \tag{1}$$

up to fourth order of the steepness kA. The coefficients $\mathfrak{F}_{mn}$ represent kernel functions corresponding to sum ($m = n$) and difference ($m-n = 2$) harmonics and $\varphi = \omega t + \varphi_0$ is the phase of the linear component of the incident wave with φ_0 a prescribed phase. The basic assumption of the harmonic decomposition technique from a nonlinear wave force is that the response follows the structure of the class Stokes expansion.

The methodology we utilise for extracting the different harmonics $\cos n\omega t$ is a phase manipulation technique presented in Fitzgerald et al. (2014) for a numerical model. The idea is to make the incident wave with a prescribed phase $\varphi_0 = 0°, 90°, 180°$ and $270°$. By linearly combining the four corresponding responses F_0, F_{90}, F_{180} and F_{270}, the separated harmonics are

$$\left(A\mathfrak{F}_{11} + A^3\mathfrak{F}_{31}\right)\cos\omega t = (F_0 - F_{90}^H - F_{180} + F_{270}^H)/4, \tag{2a}$$

$$\left(A^2\mathfrak{F}_{22} + A^4\mathfrak{F}_{42}\right)\cos 2\omega t = (F_0 - F_{90} + F_{180} - F_{270})/4, \tag{2b}$$

$$A^3\mathfrak{F}_{33}\cos 3\omega t = (F_0 + F_{90}^H - F_{180} - F_{270}^H)/4, \tag{2c}$$

$$A^2\mathfrak{F}_{20} + A^4\mathfrak{F}_{40} + A^4\mathfrak{F}_{44}\cos 4\omega t = (F_0 + F_{90} + F_{180} + F_{270})/4. \tag{2d}$$

where the accuracy is truncated to fourth order and the superscript H denotes the Hilbert transform of the time signal. Clearly, to extract the harmonics up to fourth order using this approach, one has to repeat each simulation four times with careful control of the phase of the wavemaker. Note that the harmonic terms might not be exactly the same order, for instance, Eq. (2a) is the first harmonic term but it contains a 3rd-order components $A^3\mathfrak{F}_{31}$. This difference term is two orders smaller than the sum term $A\mathfrak{F}_{11}$ thus it is not necessary to further separate them except the term $A^2\mathfrak{F}_{20}$ in (2d) which is the second order difference component. The same model applies to the wave moment.

Reconstruction model

Once we obtain the harmonic loading coefficients and the corresponding phases, it is then straightforward to reconstruct the force and moment according to the 'Stokes-like' harmonic structure. The reconstruction of the nonlinear force and moment relies on the Stokes-like model of the harmonic components. We first write the linear force component as

$$F^{(1)} = \mathcal{F}^{(1)} f_1 \tag{3}$$

where f_1 carries the group structure and phase information for the linear loading, and $\mathcal{F}^{(1)}$ carries the information of the linear force amplitude. Then the total force can be estimated as

$$\frac{F}{\rho g R^3} = \frac{\mathcal{F}^{(1)}}{\rho g R^3} f_1 + S_{FF2}\left(\frac{\mathcal{F}^{(1)}}{\rho g R^3}\right)^2 f_2 + S_{FF3}\left(\frac{\mathcal{F}^{(1)}}{\rho g R^3}\right)^3 f_3 + S_{FF4}\left(\frac{\mathcal{F}^{(1)}}{\rho g R^3}\right)^4 f_4 + S_{FF5}\left(\frac{\mathcal{F}^{(1)}}{\rho g R^3}\right)^5 f_5 \tag{4}$$

where

$$f_n = \alpha_{FFn} f_{an} + \beta_{FFn} f_{\beta n}, \quad n = 2, 3, 4, 5 \tag{5}$$

with

$$\begin{aligned}
f_{a2} &= f_1^2 - f_{1H}^2 \\
f_{\beta 2} &= 2 f_1 f_{1H} \\
f_{a3} &= f_1(f_1^2 - 2f_{1H}^2) \\
f_{\beta 3} &= f_{1H}(3f_1^2 - f_{1H}^2) \\
f_{a4} &= (f_1^2 - f_{1H}^2)^2 - (2 f_1 f_{1H})^2 \\
f_{\beta 4} &= 4 f_1 f_{1H}(f_1^2 - f_{1H}^2) \\
f_{a5} &= [(f_1^2 - f_{1H}^2)^2 - (2 f_1 f_{1H})^2] f_1 - 4 f_{1H}^2 f_1 (f_1^2 - f_{1H}^2) \\
f_{\beta 5} &= [(f_1^2 - f_{1H}^2)^2 - (2 f_1 f_{1H})^2] f_{1H} + 4 f_1^2 f_{1H}(f_1^2 - f_{1H}^2)
\end{aligned} \tag{6}$$

At each higher harmonic, S_{FFn} carries the non-dimensional force coefficient, and the phase coefficients α_{FFn} and β_{FFn} are approximated by

$$\alpha_{FFn} = \frac{\int f_n f_{an}\mathrm{d}t}{\int f_{an}^2\mathrm{d}t}, \quad \beta_{FFn} = \frac{\int f_n f_{\beta n}\mathrm{d}t}{\int f_{\beta n}^2\mathrm{d}t}. \tag{7}$$

The phase of the harmonic force relative to the linear force component is then defined as $\phi_n = \arctan(\beta_{FFn}/\alpha_{FFn})$.

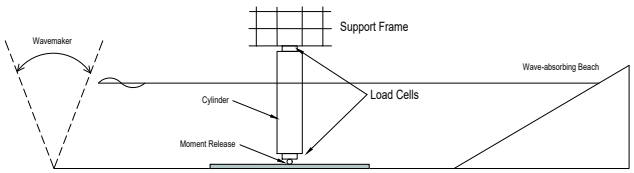

Fig. 1 The schematic overview of the experimental setup.

The moment reconstruction model is similar to the force as

$$\frac{M}{\rho g R^3 h} = \frac{\mathcal{M}^{(1)}}{\rho g R^3 h} m_1 + S_{MM2}\left(\frac{\mathcal{M}^{(1)}}{\rho g R^3 h}\right)^2 m_2 + S_{MM3}\left(\frac{\mathcal{M}^{(1)}}{\rho g R^3 h}\right)^3 m_3 + S_{MM4}\left(\frac{\mathcal{M}^{(1)}}{\rho g R^3 h}\right)^4 m_4 + S_{MM5}\left(\frac{\mathcal{M}^{(1)}}{\rho g R^3 h}\right)^5 m_5 \tag{8}$$

with S_{MMn} as the nth harmonic moment coefficient and m_n carrying the group structure and phase information. The still water depth is h.

Finally, given the effective moment arm h_n at each harmonic, one would be able to approximate the moment from the force by

$$\frac{M}{\rho g R^3 h} = \frac{h_1}{h}\frac{\mathcal{F}^{(1)}}{\rho g R^3} f_1 + S_{FF2}\frac{h_2}{h}\left(\frac{\mathcal{F}^{(1)}}{\rho g R^3}\right)^2 f_2 + S_{FF3}\frac{h_3}{h}\left(\frac{\mathcal{F}^{(1)}}{\rho g R^3}\right)^3 f_3 + S_{FF4}\frac{h_4}{h}\left(\frac{\mathcal{F}^{(1)}}{\rho g R^3}\right)^4 f_4 + S_{FF5}\frac{h_5}{h}\left(\frac{\mathcal{F}^{(1)}}{\rho g R^3}\right)^5 f_5. \tag{9}$$

EXPERIMENTAL SETUP

The experiments were undertaken at the Kelvin Hydrodynamic Laboratory in the University of Strathclyde, United Kingdom. The tests were carried out in the lab's 76 m long, 4.6 wide wave tank with a constant water depth of 1.8 m over a flat bottom. The tank is equipped with a 'flap-type' wavemaker consisting of four paddles with force-feedback at one end, and a sloping beach acting as a passive absorber at the other end. A single surface-piercing vertical cylinder of diameter 0.315 m was placed at the centreline of the tank, with its centre 35.315 m away from the wavemaker. Figure 1 shows the sketch of the experimental setup. The cylinder was rigidly supported at its upper end by a six-degree-of-freedom load cell mounted on a stiff frame. The bottom of the cylinder was fixed to a frame attached to the tank floor via a three-degree-of-freedom load cell attached to a bearing assembly which released the bending moments. The lower support raised the end of the cylinder slightly above the tank floor; the resulting cylinder draught was 1.6 m. The upper end of the cylinder is located just under 1.0 m above the still water surface, to allow for the substantial run-up of the large focused waves. The arrangement allows the calculation of the total inline force and the inline moment about the bearing, so that the moment arm may be found. Figure 2 shows a wide view of the cylinder viewed from the wavemaker as a wave passes, with the inset image showing the side view.

Before the installation of the cylinder, focused incident waves were calibrated. Wave probes were placed in the wave field near the centre of the tank. To find the accurate position of the probe located at the centre in the absence of the cylinder, a laser position indicator was installed above the tank. This was used to locate the position of the cylinder as well. Due to the nonlinear evolution of the incident waves, the focused position is usually downstream the linear focused point and is delayed in time (see Adcock et al. 2015). As wave-group evolution has significant non-linearities in unidirectional waves, iteration was used to produce the focussed wave group, although finding the accurate focusing location is not necessary for the four-phase combination technique adopted in the experiments.

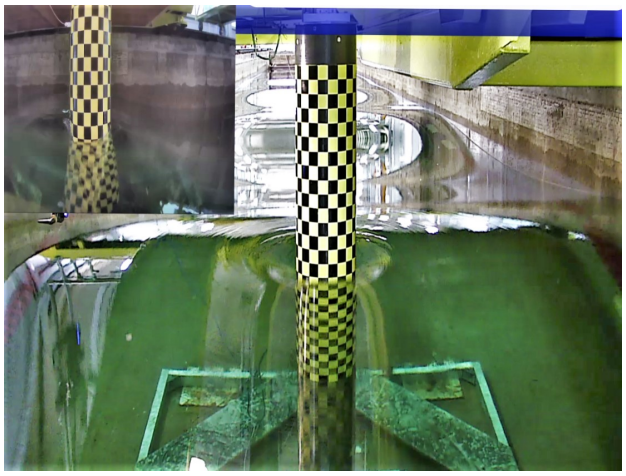

Fig. 2 The experimental setup in the Kelvin Hydrodynamic Laboratory, a wave crest past the cylinder.

Table 1 Test parameters.

Case	$f_p(Hz)$	k_pR	k_ph	$A(m)$	k_pA	KC
1	0.429	0.129	1.476	0.134	0.110	2.671
2	0.429	0.129	1.476	0.147	0.120	2.927
3	0.429	0.129	1.476	0.160	0.131	3.185
4	0.429	0.129	1.476	0.169	0.138	3.366
5	0.429	0.129	1.476	0.179	0.146	3.562
6	0.429	0.129	1.476	0.206	0.169	4.110
7	0.429	0.129	1.476	0.241	0.197	4.802
8	0.429	0.129	1.476	0.256	0.210	5.115

The JONSWAP spectrum of peak frequency f_p with $\gamma = 3.3$ was used to generate the wave groups. The discretized spectrum cut-off is set as $0.5f_p - 3.0f_p$. The tested wave groups were listed in Table 1. k_p for the wave group is the peak wavenumber. Amplitude $A(m)$ is the linear component of the focused wave group. KC is computed by $KC = \pi A/R$.

The test condition gives a range of the ratio A/R = (0.6 - 1.9), that is, the wave group amplitude is mostly of the same order with the cylinder radius where FNV model for third-order force should apply. The corresponding wave steepness k_pA is (0.10 - 0.25) and no wave breaking is expected in this range. With the KC number smaller than 5 (except Case 8), we expect the wave force is inertia dominant. Local viscous effects might play a role when $KC > 4.0$.

RESULTS

Harmonic decomposition

Experiment

Using the phase manipulation technique described previously, We can separate the harmonics at least up to the first four orders. Figure 3 shows the time histories of wave induced moment about the bottom bearing on the cylinder for the decomposed harmonics near the focusing time. It is clear that the linear and second harmonic components are easily recognized. The linear moment is symmetric about the focusing time

near 64 s. The second harmonic is double the linear frequency and makes a significant contribution as compared with the linear component. The third and fourth harmonics are relatively small.

In order to identify further higher harmonics, we transfer the time histories to the frequency domain. Figure 4 shows the decomposed spectra of horizontal wave moment for Case 8 with $A = 0.256$ m or $k_pA = 0.21$. The frequency is normalized by the peak frequency in the horizontal axis. The vertical axis measured value is plotted in log scale. The linear moment corresponding to the linear free wave component is between $0.5f_p - 3f_p$ in the black line, while the second harmonic is between $1.0f_p - 5f_p$ in the red line. The second difference component is between $0.0f_p - 2.0f_p$ in the blue line, which can be easily separated from the fourth harmonic. It is seen that the separation is clean up to even $16f_p$. There is a small amount of 'leakage' between components – for instance a peak in most components can be seen around $f/f_p = 1$. However, this leakage is typically small and can be removed by filtering in the frequency domain. This clean separation of the higher harmonics demonstrates the successful application of the phase manipulation approach in decomposing harmonic loads on the structure in the experiments.

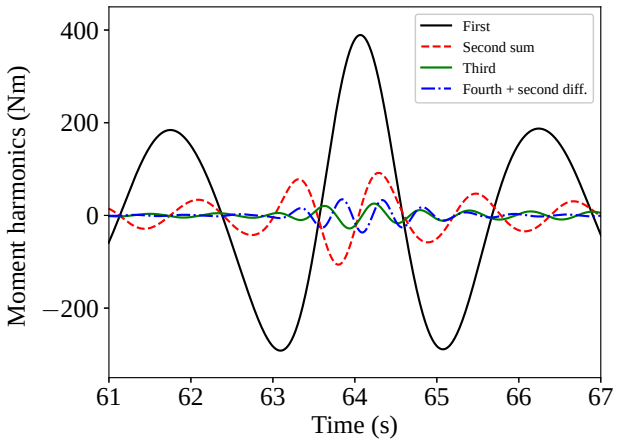

Fig. 3 Decomposed time histories of wave moment for Case 8, $k_pR = 0.129$ and $k_pA = 0.21$.

Numerical simulatioin

We employ a rectangular numerical wave tank model for studying the nonlinear wave structure interactions. The numerical model is based on the fully nonlinear potential flow theory and employs a higher-order boundary element methods to solve the boundary value problem. Detailed description of the numerical wave tank and relevant validation was reported recently in Feng et al. (2019). Specifically, the numerical model is a representation of the physical tank, with similar mechanism of wave generation and wave absorption. The model is developed in the framework of potential flow so that no viscous effects are present. Anything nonlinear produced in the simulation can be associated with nonlineraity in the free-surface boundary conditions.

Phase control is implemented in the model to apply the phase manipulation approach as in the experiment. Figure 5 shows the decomposed wave moment spectra against the normalized frequency. Again the separation among harmonics are excellent. The numerical results are

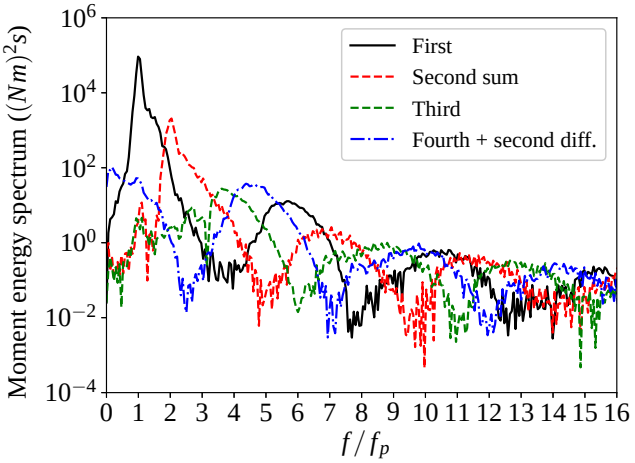

Fig. 4 Energy density spectra of wave moment for for Case 8, $k_pR = 0.129$ and $k_pA = 0.21$. $M/rhogAR^2h$

shown only up to the ninth harmonics unlike in the experiments. The accuracy of numerical results is limited by the mesh resolution used for the boundary discretization. As the value of the harmonics higher than the fifth or sixth and the corresponding wavelength of the component is very short, extremely high mesh resolution would be needed to capture those components. Considering the efficiency of simulations, we apply a reasonable resolution for our model such that the accuracy is reliable up to the fifth harmonic. We see in Figure 5 that beyond $f/f_p = 6$ the spectrum values become messy and overlapping among different components.

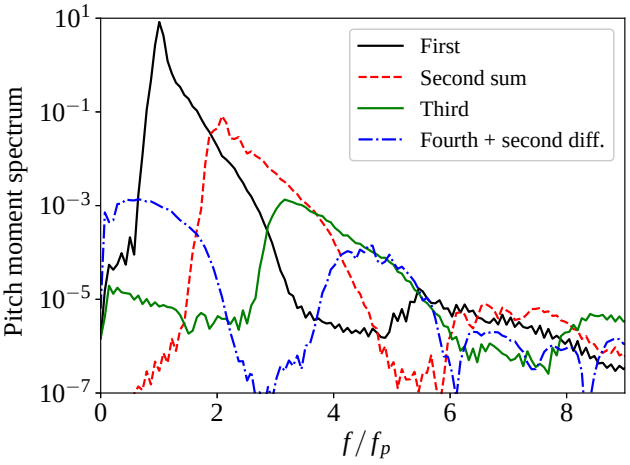

Fig. 5 Energy density spectra of wave moment for numerical simulation, $k_pR = 0.129$ and $k_pA = 0.1$. The moment is nondomensionalized by $M/\rho gAR^2h$.

With such cleanly separated spectra, it is easy to utilize appropriate bandpass frequency filters to extract the harmonics. Figure 6 presents the bandpass functions we used for extraction of the second to fifth harmonics. The shape of the filtering functions follow more or less the

profile of the its corresponding spectra profile – a steep rise and a mild long tail. Applying these filters to Figure 7 produces the results.

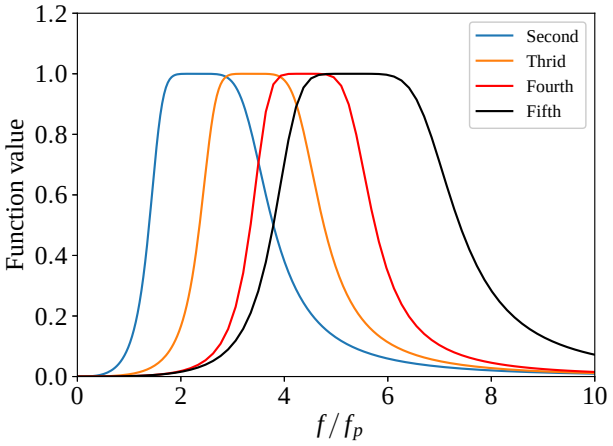

Fig. 6 Bandpass filtering function used for extracting harmonics from decomposed time histories.

Figure 7 summaries the results in the time domain for a typical case from our numerical simulations. It shows the time histories of wave moment of each harmonic up to the fifth. The moment is non-dimensionalized by $\rho g A R^2 h$. For the linear (first order) moment, it can be seen that it has a similar shape to the NewWave profile. We also plot the envelope of the time history, from the time-history data and its Hilbert transform as $M_A(t) = \sqrt{M_1^2(t) + M_{1H}^2(t)}$, where M_{1H} is the Hilbert transform of the linear moment. The second order difference component is small but shows a larger skew profile near focusing time. It might be a combination of the load due to the second order free long wave and a larger skew-symmetric loading due to the return current under the wave-group. Higher harmonics appear to be extracted cleanly with some additional structure discernible at the 5th harmonic. The approximated envelopes of the n^{th} ($n > 1$) harmonics are calculated by raising the linear envelope to the power of n and scaling to the magnitudes of the corresponding harmonics. The scaling is based on the peak value of the component. It can be seen that the n^{th} powered envelopes agree very well with the extracted harmonic time histories, both the shape in time and the timing of the peak of the envelops. This is consistent with the assumed 'Stokes-type' wave load harmonic structure. This structure provides the basis to predict the higher harmonic loads using only the linear component.

Nonlinear effects

The effects of nonlinearity on higher-order harmonic loads can be evaluated by increased incident wave steepness. The non-dimensionalized loads gives better understanding of the nonlinear effects. We apply the scaling introduced by Huseby and Grue (2000), that is, the n^{th} harmonic is non-dimensionalized as $F^{(n)}/\rho g A^n R^{(3-n)}$ for the force, and for the n^{th} harmonic of moment we use $\rho g A^n R^{3-n} h$ which adds the mean water depth to the scaling of force. Here we choose to analyse the moment acting around the base of the column (i.e. the 'mudline') as this is of most significance to practical engineering design. The variation of the harmonic moment (peaks) with increased wave steepness is shown in Figure 8. Four cases of wave steepness ranging 0–0.1 are studied. Peak values of the envelopes of the moments harmonic are extracted as described above.

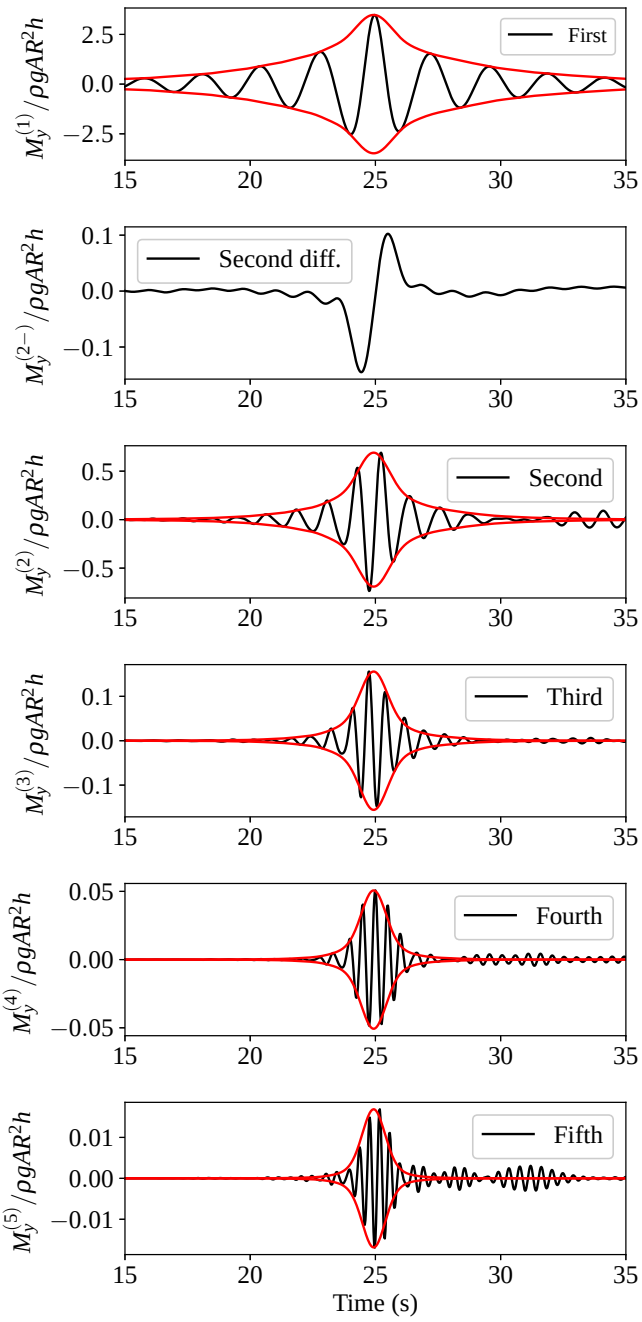

Fig. 7 Harmonic components of wave moment from numerical simulations for Case 8, $k_pR = 0.129$ and $k_pA = 0.1$. The envelopes of the components are in solid red. The linear envelope is directly computed from its time history. Envelopes of higher harmonics are obtained by raising the linear envelope to n^{th} power and scaling to its magnitude.

We see in Figure 8 that the non-dimensionalized linear moment coefficient remains almost constant over the k_pA range. Linear results computed by the Morison inertial formula and by MacCamy-Fuchs' formula are also included. The theoretical results for linear moment are not a function of wave steepness, such that they are constant across

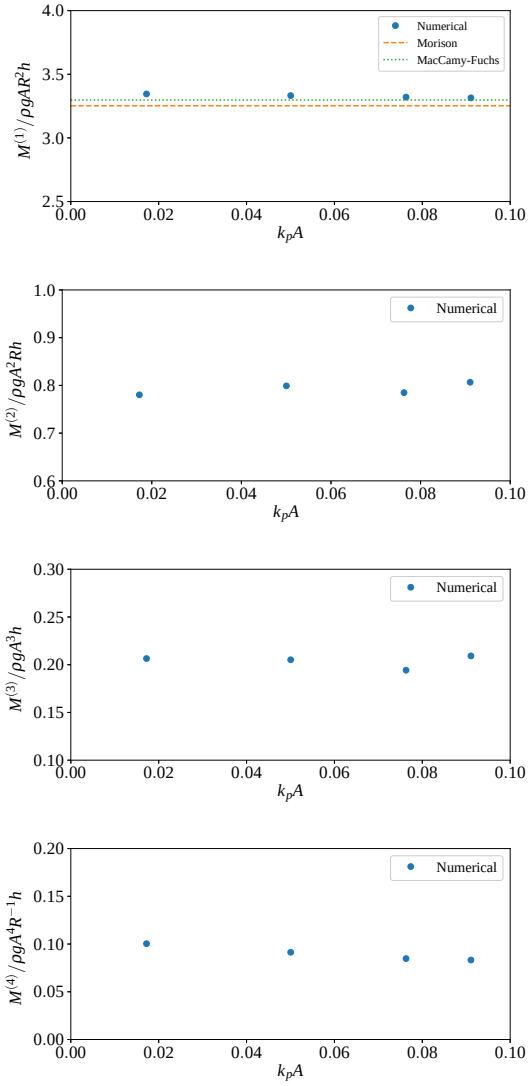

Fig. 8 Numerical results: variation of peak harmonic mudline moments with increasing wave steepness k_pA. The n^{th} harmonic moment $M^{(n)}$ is non-dimensionalized by $\rho g A^n R^{(3-n)} h$.

the steepness range. The agreement is very good for the results from our numerical simulation and theoretical predictions. Note that as the cylinder in our study is compact (slender cylinder), Morison's equation remains valid.

The non-dimensional second harmonic moments from the numerical simulations show very small variation as the wave steepness increases. The third and fourth harmonic moments are again almost constant. These non-dimensional harmonic moments are indeed the coefficients in Eq. (8). They are useful for reconstructing the harmonic moments at any wave steepness, given the underlying group structure and phase.

To understand the moment values further, it is useful to consider an effective point on the cylinder at which the harmonic force 'acts'. The force is, of course, oscillatory and therefore we consider the ratio of the envelope of the moment to the envelope of the force,

$$L_n = \frac{\max(\sqrt{M_n^2 + M_{nH}^2})}{\max(\sqrt{F_n^2 + F_{nH}^2})}, \tag{10}$$

and we use the maximum values of envelopes of the harmonic moment and force. L_n is defined as the effective moment arm at nth harmonic. Both the experimental and numerical results show that the linear force 'acts' at about 0.5 m below the still water surface or the linear moment arm is about 1.3 m, above the tank bottom. The second harmonic force 'acts' slightly below the water surface. More interesting is that, harmonic forces higher than the third are mostly near the undisturbed free surface, which give the moment arms as the water depth. With these moment arms, we can approximate the higher harmonic moments from only the linear force, as demonstrated in Eq. (9).

Nonlinear load reconstruction

The harmonic decomposition utilised in this study should allow a non-linear force time series to be reconstructed given a known linear loading. It is assumed that the linear loading is relatively straightforward to calculate: for a sufficiently compact cylinder the linear inertia component in the Morison equation or from the McCamy-Fuchs expression for slightly larger cylinders. To use the present approach for the harmonics, amplitude and phase coefficients for higher harmonics are needed. These values are obtained from the experiments or numerical simulations. An advantage is, the relevant coefficients are shown not to be a function of wave steepness as demonstrated previously. This implies that we should be able to use the same set of non-dimensional coefficients for prediction of the case at a steeper wave condition.

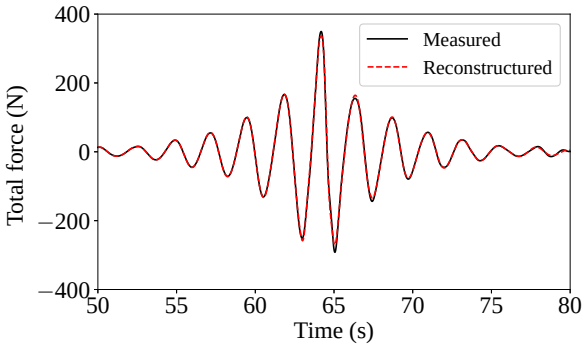

Fig. 9 Reconstruction of nonlinear force for Case 8, $k_pR = 0.129$ and $k_pA = 0.21$.

As a check on the consistency of the approach taken in the present study, we now use this approach to reconstruct the force and moment time histories from only the linear time histories and the non-dimensional coefficients. Figure 9 shows the reconstructed force which is in almost perfect agreement with that measured. Figure 10 presents moment of numerical simulation for Case 8. The averaged values of the coefficients in Figure 8 are used for the reconstruction, based on the 'Stokes-like' harmonic structure. The total moment reconstructed, the top panel figure, is very close to the simulated results. The time history only shows a small discrepancy around the crests and troughs either side of the main crest. We also include a reconstruction of the different individual harmonics. Overall, the reconstruction for the harmonic moments are

pretty successful. Given that the nonlinear loads follow the Stokes-like harmonic structure, it is practically useful to approximate higher harmonic force and moment on the offshore wind turbine monopile in a simple manner without performing nonlinear diffraction analysis.

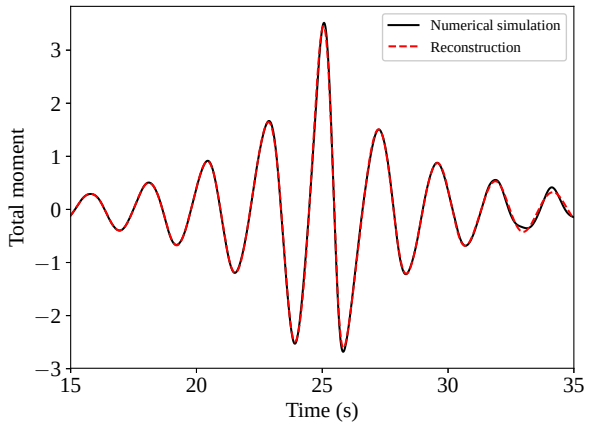

Fig. 10 Reconstruction of moment of numerical simulation for $k_pR = 0.129$ and $k_pA = 0.1$.

CONCLUSIONS

In this work we have investigated the higher harmonics of moments acting on an inertia dominated surface-piercing cylinder. Both experimental and numerical results are obtained and carefully analyzed. For cylinders in the 'inertia' range, a Stokes-like model of harmonics for both force and overturning moment appears to work well.

We focus on the moment on the cylinder. The moment is known to be more non-linear than force (i.e. higher harmonics are relatively larger) as the higher harmonics effectively act higher up the cylinder. The experimentally obtained moment arm confirms that these higher (than the second) harmonics 'act' near the free surface. We demonstrate that with the harmonic load coefficients and their phases, the time histories of these harmonics can be successfully reconstructed following the Stokes-like structure. The simple Stokes-like model for higher harmonics presented in this paper is a good model for loading on a slender cylinder. The model does capture much of the structure of the higher harmonics and as such we believe it can serve as a useful, practical engineering model.

ACKNOWLEDGEMENT

This work was funded by UK/China ORE funding (EPSRC grant EP/R007632/1) and the United Kingdom Centre for Marine Energy Research (UKCMER) (EPSRSC grant P/R007632/1). The authors would also like to acknowledge the use of the University of Oxford Advanced Research Computing (ARC) facility in carrying out the numerical work.

REFERENCES

Adcock, TAA, Taylor, PH, Draper, S (1995). "Nonlinear dynamics of wave-groups in random seas: unexpected walls of water in the open ocean", *Proc of R Soc A*, No 471, pp 20150660.

Chaplin, JR, Rainey, RCT, Yemm, RW (1997). "Ringing of a vertical cylinder in waves", *Journal of Fluid Mechanics*, No 350, pp 119–147.

Chen, LF, Zang, J, Taylor, PH, Sun, L, Morgan, GCJ, Grice, J, Orszaghova, J, Tello Ruiz, M (2018). "An experimental decomposition of nonlinear forces on a surface-piercing column: Stokes-type expansions of the force harmonics", *Journal of Fluid Mechanics*, No 848, pp 42–77.

Davies, KB, Leverette, SJ, Spillane, MW (1994). "Ringing response of TLP and GBS platforms", *Proceedings of 7th Intl Conf on the Behaviour of Offshore Structures, Cambridge, USA*, No pp 569–585.

Faltinsen, OM, Newman, JN, Vinje, T (1995). "Nonlinear wave loads on a slender vertical cylinder", *Journal of Fluid Mechanics*, No 289, pp 179–198.

Feng, X, Willden, RH, Zhou, B, Adcock, TAA (2019). "Numerical analysis of nonlinear wave loads on an offshore wind turbine monopile", *Proc of the 38th Intl Conf on Ocean, Offshore and Arctic Engineering, Glasgow, UK*.

Fitzgerald, CJ, Taylor, PH, Eatock Taylor, R, Grice, J., Zang, J (2014). "Phase manipulation and the harmonic components of ringing forces on a surface-piercing column", *Proc of R Soc A*, No 470, pp 20130847.

Huseby, M, Grue, J (2000). "An experimental investigation of higher-harmonic wave forces on a vertical cylinder", *Journal of Fluid Mechanics*, No 414, pp 75–103.

Kallehave, D, Byrne, BW, Thilsted, CL, Mikkelsen, KK (2015). "Optimization of monopiles for offshore wind turbines", *Phil. Trans. R. Soc. A*, No 373, pp 20140100.

Kristiansen, T, Faltinsen, OM (2017). "Higher harmonic wave loads on a vertical cylinder in finite water depth", *Journal of Fluid Mechanics*, No 833, pp 773–805.

Krokstad, JR, Stansberg, TC (1995). "Ringing load models verified against experiments", *Proc of the 14th Intl Conf on Ocean, Offshore and Arctic Engineering, Copenhagen, Denmark*, pp 223–234.

Malenica, S, Molin, B (1995). "Third-harmonic wave diffraction by a vertical cylinder", *Journal of Fluid Mechanics*, No 302, pp 203–229.

Rainey, RCT (1989). "A new equation for calculating wave loads on offshore structures", *Journal of Fluid Mechanics*, No 204, pp 295–324.

Rainey, RCT (1995). "Slender-body expressions for the wave load on offshore structures", *Proc of R Soc Lon A*, No 450, pp 391–416.

Riise, BH, Grue, J, Jensen, A (2018). "High frequency resonant response of a monopile in irregular deep water waves", *Journal of Fluid Mechanics*, No 853, pp 564–586.